**Astronomy
&
Astrophysics**

A forming disk at $z \sim 0.6$:
collapse of a gaseous disk or major merger remnant?

M. Puech[1,2], F. Hammer[2], H. Flores[2], B. Neichel[2], and Y. Yang[2]

[1] ESO, Karl-Schwarzschild-Strasse 2, 85748 Garching bei München, Germany
e-mail: mpuech@eso.org
[2] GEPI, Observatoire de Paris, CNRS, University Paris Diderot, 5 place Jules Janssen, 92190 Meudon, France

ABSTRACT

Context. Local spiral galaxies contain roughly two-thirds of the present-day stellar mass density. However, the formation process of disks is still poorly understood.

Aims. We present and analyze observations of J033241.88-274853.9 at $z = 0.6679$ to understand how its stellar disk was formed.

Methods. We combine multi-wavelength EIS, HST/ACS, Spitzer/IRAC, and GALEX imaging with FLAMES/GIRAFFE 3D spectroscopy to study its color-morphology and spatially-resolved kinematics. A spectral energy distribution (SED) is constructed and physical properties extracted using stellar population models.

Results. J033241.88-274853.9 is a blue, young (320^{+590}_{-260} Myr, 90% confidence interval) stellar disk embedded in a very gas-rich ($f_{gas} = 73-82\%$ with $\log(M_{stellar}/M_{\odot}) = 9.45\pm^{0.28}_{0.14}$) and turbulent phase that is found to be rotating on large spatial scales. We identified two unusual properties of J033241.88-274853.9. (1) The spatial distributions of the ionized gaseous and young stars show a strong decoupling; while almost no stars can be detected in the southern part down to the very deep detection limit of ACS/UDF images (accounting for the light spread by seeing effects), significant emission from the [OII] ionized gas is detected. (2) We detect an excess of velocity dispersion in the southern part of J033241.88-274853.9 in comparison to expectations from a rotating disk model.

Conclusions. We considered two disk formation scenarios, depending on the gaseous phase geometry. In the first one, we examined whether J033241.88-274853.9 could be a young rotating disk that has been recently collapsed from a pre-existing, very gas-rich rotating disk. This scenario requires two (unknown) additional assumptions to explain the decoupling between the distribution of stars and gas and the excess of velocity dispersion in the same region. In a second scenario, we examine whether J033241.88-274853.9 could be a merger remnant of two gas-rich disks. In this case, the asymmetry observed between the gas and star distributions, as well as the excess of velocity dispersion, find a common explanation. Shocks produced during the merger in this region can be ionized easily and heat the gas while preventing star formation. This makes this scenario more satisfactory than the collapse of a pre-existing, gas-rich rotating disk.

Key words. galaxies: evolution – galaxies: kinematics and dynamics – galaxies: high-redshift – galaxies: general – galaxies: spiral – galaxies: interactions

1. Introduction

While the majority of the local stellar mass density is locked into spiral galaxies, our understanding of the formation of galactic disks still remains incomplete (Mayer et al. 2008). It has been suggested that a large fraction of local disks could have been rebuilt subsequent to a major merger since $z = 1$, owing to the remarkable coincidence of the evolution of the merger rate, morphology, and fraction of actively star-forming galaxies (Hammer et al. 2005). At first sight, this "spiral rebuilding" scenario might seem inconsistent with numerical simulations, which often predict that the product of a major merger between two spirals is an elliptical galaxy. However, it has also been shown that gas expelled in tidal tails during the merger can be re-accreted and reform a disk after such an event (Barnes 2002). More recently, theoretical and numerical clues to the disk-rebuilding hypothesis have been accumulated (Robertson et al. 2006; Lotz et al. 2008; Hopkins et al. 2008).

In the framework of an ESO large program called IMAGES ("Intermediate-MAss Galaxy Evolution Sequence", Ravikumar et al. 2007; Yang et al. 2008, hereafter Paper I), we have been gathering multi-wavelength data on a representative sample of emission line, intermediate-mass galaxies at $z \sim 0.6$, i.e., 6 Gyr ago. These galaxies are the progenitors of present-day spirals, which contain approximately two-thirds of the present-day stellar mass density (Hammer et al. 2007). In Paper I, we presented the GIRAFFE spatially resolved kinematics of this sample of 65 galaxies. In Neichel et al. (2008) (hereafter Paper II), we studied in detail their color-morphology using HST/ACS multi-wavelength imaging. In Puech et al. (2008) (Paper III), we analyzed their dynamical properties through the evolution of the near-infrared Tully-Fisher relation. This series of papers has revealed a surprisingly high fraction of kinematically nonrelaxed galaxies (Paper I), while well-relaxed spiral rotating disks appear to be evolving since $z \sim 0.6$, i.e., over the past 6 Gyr, by a factor as much as two, both in number (Paper II) and stellar mass (Paper III). Clearly, the spiral-disk galaxy history over the last 6 Gyr seems to be particularly agitated, much more than initially thought.

Space imaging combined with ground-based 3D spectroscopy can reveal the physical processes at work in such distant galaxies with unprecedented detail (Puech et al. 2007b). In the present letter, we present another spin-off of the IMAGES Large Program, which is a very young ($\sim$300 Myr old) rotating disk
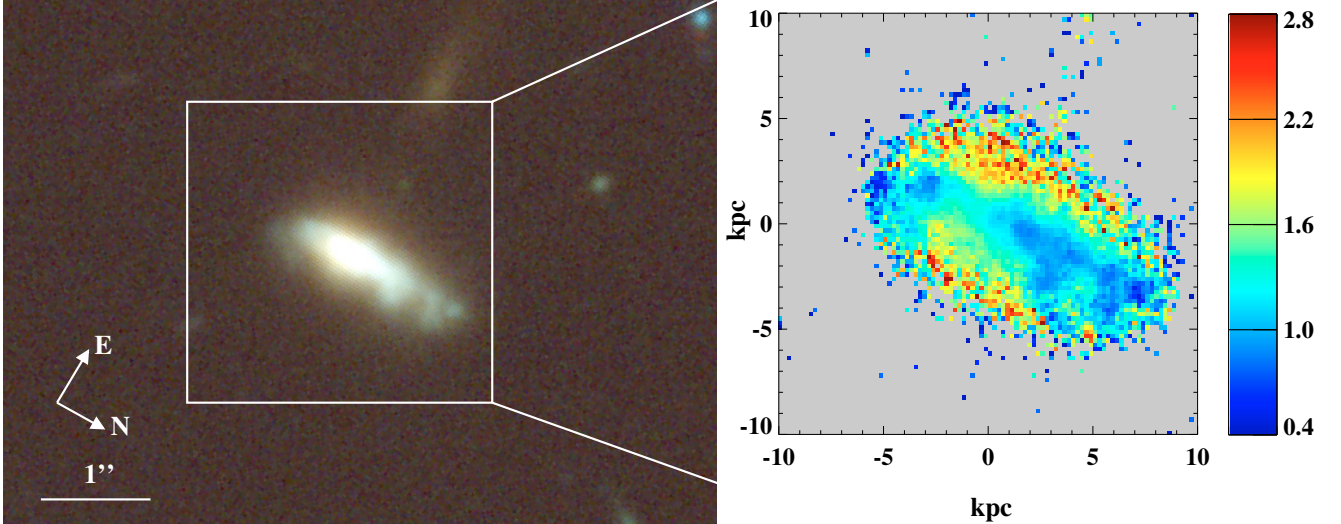
Fig. 1. *Left*: HST/ACS $B - V - z$-band image of J033241.88-274853.9 form the Hubble Ultra-Deep Field (0.03 arcsec/pix, Beckwith et al. 2006). *Right*: $B - z$ color map.
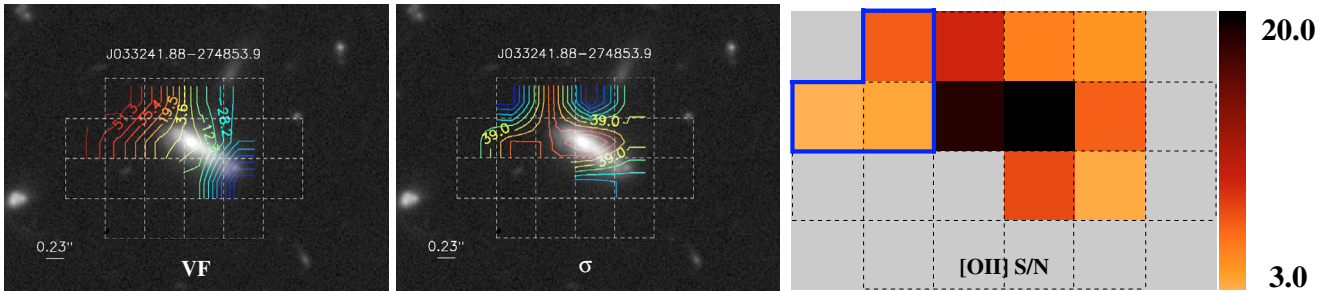

Fig. 2. $B + V + z$ image of J033226.23-274222.8 superimposed with GIRAFFE data. In *the left and middle panels*, the IFU bundle is overlaid in white dash lines (0.52 arcsec/pix), and the residual uncertainty on the alignment between the images and the IFU is shown as an horizontal white bar in the lower-left corner. *Left panel*: isovelocities have been superimposed, with contours approximately ranging from -90 to $60 \, \text{km s}^{-1}$ by steps of $8 \, \text{km s}^{-1}$. A $S/N = 3$ threshold is used to limit measurement uncertainties, which explains why kinematical data do not extent over the whole IFU FoV. *Middle panel*: GIRAFFE velocity dispersion map contours, ranging from 27 to 47 km s^{-1} by steps of $2 \, \text{km s}^{-1}$. *Right panel*: [OII] emission Signal-to-Noise map in GIRAFFE IFU pixels. Pixels where no stellar light has been detected in ACS images are ensquared in blue.

captured during its formation process. This article is organized as follows: Sect. 2 presents the morphological and kinematic properties of J033241.88-274853.9, Sect. 3 its SED fitting, and Sect. 4 the derivation of its stellar mass and star formation rate. Section 5 presents two possible scenarios of disk formation. A discussion and conclusion are given in Sect. 6. Throughout, we adopt $H_0 = 70 \, \text{km s}^{-1} \, \text{Mpc}^{-1}$, $\Omega_M = 0.3$, and $\Omega_\Lambda = 0.7$, and the *AB* magnitude system.

2. Morpho-kinematics

Figure 1 shows a large view of J033241.88-274853.9, which reveals a relatively edge-on Peculiar/Tadpole galaxy (see Paper II): J033241.88-274853.9 appears to be very asymmetric with a more elongated side toward North. This tail shows several blue regions with $B - z$ colors typical of star-bursting galaxies, while the overall color is representative of late-type galaxies ($B - z = 1.3$, see Paper II). The reddish edges of J033241.88-274853.9 suggests a moderate presence of dust in this galaxy.

The stellar light distribution of J033226.23-274222.8 was analyzed using a two-component Sersic decomposition on the z-band image with GALFIT (Peng et al. 2002). We required these two components to be both centered on the dynamical/continuum center of the galaxy (see below) and masked the

southern part J033241.88-274853.9 to fit only the northern region in order to be able to reproduce its asymmetry. We found Sersic indexes $n = 0.34$ and $n = 0.54$ for the outer and inner components respectively, with an inner-to-outer light ratio ~ 0.12. This suggests that J033241.88-274853.9 is composed of an inner symmetric stellar disk embedded in another bluer extended "half-disk".

In Fig. 2, we have superimposed the GIRAFFE velocity Field [VF] and the velocity dispersion-map [σ-map] to the ACS imaging (see Puech et al. 2007b, for detail). An additional correction was performed by eye, by aligning the B-band HST/ACS image and the [OII] emission line distribution (not shown here), since in principle they both trace the spatial distribution of O/B blue giant stars. Aligning the peaks of both distributions, we ended up with an additional shift of 0.2 arcsec in RA and 0.03 arcsec in Dec, i.e., smaller than the residual uncertainty of the astrometric alignment (0.23 arcsec). No large-scale perturbation can be seen in the kinematics of J033241.88-274853.9, which was classified as a rotating disk in Paper I. The central peak in the σ-map is well reproduced by a rotating disk model and indicates the position of the dynamical center of rotation, which matches relatively well the continuum peak (see Fig. 2 and Paper I). One can however note that this central peak of dispersion has two extensions in the southern part, which are

not reproduced by the rotating disk model of Paper I. Moreover, the gaseous phase in J033241.88-274853.9 has a relatively low $V/\sigma = 3.79 \pm 0.94$ value, which is among the lowest values found in the sample of distant rotating disks (Puech et al. 2007a). Such a value is lower than the local median and, together with the two extensions of the dispersion peak, it suggests than the ionized gas in the southern part of J033241.88-274853.9 is relatively turbulent. We will discuss further the excess of velocity dispersion relative to a rotating disk model in Sect. 5.

Of importance, GIRAFFE detected [OII] emission on the southern side, where no stellar emission can be detected, even in the very deep ACS images of the HUDF (10-σ detection limit of $V_{AB} = 29.3$ mag/arcsec^2 in the 0.52×0.52 arcsec^2 GIRAFFE IFU pixel aperture, see the [OII] S/N map in Fig. 2). Such an asymmetry between gas and star distributions is unusual. We used a VIMOS spectrum of J033241.88-274853.9, retrieved from the VVDS (Le Fèvre et al. 2005, see Fig. 6), and the GIRAFFE [OII] emission map to estimate the [OII] flux in the leftest GIRAFFE pixel. We degraded the V-band ACS image down to the spatial resolution and sampling of GIRAFFE observations to estimate the rest-frame pseudo-continuum around the [OII] emission line. We were then able to roughly estimate the rest-frame [OII] equivalent width in this pixel, which was found to be $EW_0([OII]) = 140$ Å. We will discuss this point in Sect. 5.

3. Spectral energy distribution

We gathered photometric measurements of J033241.88-274853.9 in constant apertures of 3 arcsec in diameter, as shown in Fig. 3. We distinguished between space-based measurements, in green, and ground-based measurements, in black. Space-based measurements correspond to, from the UV to the IR, GALEX/NUV (Morrissey et al. 2007), HST/ACS (F435W [B], F606W [V], F775W [i], and F850LP [z] Beckwith et al. 2006), and Spitzer/IRAC (3.6, 4.5, 5.8, and 8.0 μm, Dickinson et al., in prep.), while ground-based measurements correspond to EIS (U', U, B, V, R, and I bands in the optical, Arnouts et al. 2001), and GOODS-ISAAC (J, H, and K_S bands, Vandame et al., in prep.) in the NIR. Because of the large uncertainty associated with the zero point calibration of the GOODS H-band, we used the revised calibration proposed by Wuyts et al. (2008). Finally, J033241.88-274853.9 was neither detected by GALEX in the FUV (the 5-σ detection limit is represented as a vertical arrow), Spitzer/MIPS in the Far-Infrared (Chary et al., in prep.), or CHANDRA in X-rays (Giacconi et al. 2002; Rosati et al. 2002).

Full horizontal error-bars represent the FWHM of the photometric filters used in the corresponding surveys, while vertical error-bars represent the convolution of two terms, i.e., the magnitude error as given by Sextractor (Bertin & Arnouts 1996), and the systematic error associated with the uncertainty on the zero point calibration. Because of the very large size of both the GALEX PSF and IRAC PSF in comparison to the photometric aperture, direct photometric measurements were corrected by 2.09 mag in the NUV, following (Morrissey et al. 2007), and 0.35, 0.38, 0.51, 0.54 mag in the four respective IRAC IR bands, as directly estimated from the theoretical IRAC PSF[1]. We estimated the uncertainties associated with these PSF corrections by re-deriving these corrections in apertures of 3 arcsec modulo one PSF pixel, and added them in quadrature with other sources of uncertainty. Photometric measurements and uncertainties are listed in Table 1.
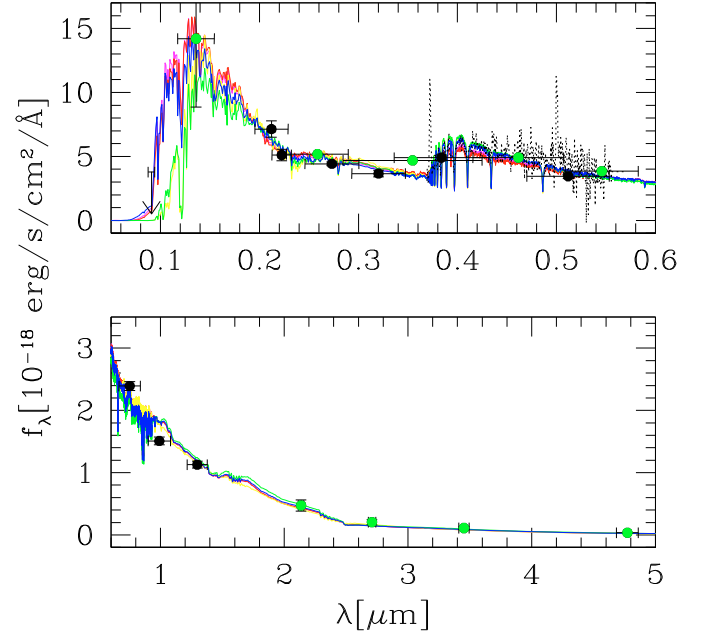
---

[1] http://ssc.spitzer.caltech.edu/irac/psf.html

Fig. 3. Rest-frame SED of J033241.88-274853.9 (3-arcsec fixed aperture photometry). Green points represent space-based photometry, while black-points represent ground-based photometry. The GALEX/FUV 5-σ detection limit is represented as a vertical arrow. A VIMOS spectrum is overlaid using a black dashed line (see also Fig. 6). Several stellar population models are shown, all acceptable within a 90% confidence interval (see text): a CSP with $Z = Z_\odot$, $\tau = 0.1$ Gyr, $t = 0.32$ Gyr, and $A_V = R_V E(B - V) = 0.28$ (best fit, blue curve), a SSP with $Z = Z_\odot$, $t = 0.1$ Gyr, and $A_V = 0.07$ (green curve), a CSP with $Z = Z_\odot$, $\tau = 0.5$ Gyr, $t = 0.64$ Gyr, and $A_V = 0.2$ (magenta curve), a SSP with $Z = 2.5\ Z_\odot$, $t = 0.09$ Gyr, and $A_V = 0.7$ (yellow curve), and a CSP with $Z = Z_\odot$, $\tau = 0.35$ Gyr, $t = 0.18$ Gyr, and $A_V = 0.8$ (red curve).

The resulting SED of J033241.88-274853.9 shows a globally declining curve from the UV to the IR (see Fig. 3). While the optical part of the SED is roughly compatible with that of an late-type galaxy (e.g., the observed $B-z$ color, see Sect. 2, which approximately corresponds to a rest-frame $\sim$2800-V color), its UV part shows an excess of light that is produced by massive blue stars (O/B), and certainly indicates a recent burst of star formation in the blue regions described in Sect. 2 (see Fig. 1).

We used Charlot & Bruzual models (Charlot & Bruzual 2007, in prep.; Bruzual 2007) to fit this SED: we assumed a Salpeter IMF (Salpeter 1955) and constructed grids of metallicity (0.005, 0.02, 0.2, 0.4, 1.0, 2.5, 5.0 $Z_\odot$), τ-exponentially declining star formation histories spaced at 0.1 Gyr intervals from $\tau = 0$ (pure SSP) to 0.5 Gyr, and at 0.5 Gyr intervals beyond, and age t. Dust was accounted for using a Cardelli et al. (1989) extinction curve parametrized by $E(B - V)$ and R_V, which was allowed to range between 2 and 6, i.e. typical values found in local group galaxies (e.g., Fitzpatrick & Massa 2007). For convenience, this extinction curve was extrapolated in the IR and the FUV. We checked that the results were not significantly changed assuming another extinction curve such as the one of Fitzpatrick (1999) or Calzetti et al. (2000).

We searched for the best model using a classical χ^2 optimization. Several well-known difficulties are associated with this procedure (e.g., Papovich et al. 2001): (1) the photometric uncertainties are often under-estimated; (2) additional systematics arise from mismatches between models and reality (e.g., wrong dust model, IMF, or star formation history, finite grid of parameters for the models, etc.); (3) the influence of

Table 1. Photometric measurements for J033241.88-274853.9. *From left to right*: 3-arcsec aperture photometry, random errors as given by Sextractor, systematic uncertainties associated with the calibration of the zero point, and uncertainties associated with the PSF-size correction (see text).

Filter	Magnitude (AB)	Random error	ZP errors	PSF errors	Total uncertainty
FUV_{GALEX}	<25.8	–	–	–	–
NUV_{GALEX}	23.49	0.12	0.03	0.38	0.40
U'_{EIS}	23.27	0.05	0.083	0.0	0.10
U_{EIS}	23.53	0.05	0.083	0.0	0.10
B_{UDF}	23.19	0.004	0.005	0.0	0.006
B_{EIS}	23.24	0.02	0.029	0.0	0.04
V_{EIS}	23.10	0.04	0.066	0.0	0.08
V_{UDF}	22.61	0.0015	0.005	0.0	0.005
R_{EIS}	22.39	0.02	0.048	0.0	0.05
I_{EIS}	22.15	0.03	0.044	0.0	0.05
I_{UDF}	21.99	0.0010	0.005	0.0	0.005
z_{UDF}	21.89	0.0016	0.005	0.0	0.005
J_{GOODS}	21.71	0.01	0.03	0.0	0.03
H_{GOODS}	21.61	0.02	0.04	0.0	0.05
K_{GOODS}	21.34	0.02	0.05	0.0	0.05
$3.6\,\mu m_{IRAC}$	21.20	0.2	0.02	0.04	0.21
$4.5\,\mu m_{IRAC}$	21.59	0.2	0.02	0.04	0.21
$5.8\,\mu m_{IRAC}$	21.73	0.2	0.02	0.03	0.20
$8.0\,\mu m_{IRAC}$	22.26	0.2	0.02	0.03	0.20

non-Gaussian errors can bias the χ^2 optimization. To check that (1) cannot impact severely our results, we compared our photometric measurements to those made in similar bands by Wuyts et al. (2008) in 2 arcsec apertures, given in their FIREWORKS catalog. We found that the SED derived from FIREWORKS is, as expected, shifted toward fainter magnitudes (by roughly ~0.1 mag), and that additional variations are well within the adopted uncertainties, which means that the adopted error-bars are not too severely underestimated. Moreover, during the fitting procedure, we enlarged the total photometric uncertainties by propagating the uncertainty associated with the center of the filter (i.e., horizontal error-bars in Fig. 3). This allowed us to take into account the additional uncertainty associated with the projection of the models onto the photometric filters, which also help mitigate against (2). Confidence intervals at 68% and 90% were determined using constant χ^2 bounds, following Avni (1976).

The best fit was found for a CSP with $Z = Z_\odot$, $\tau = 0.1$ Gyr, $t = 0.32$ Gyr, and $A_V = R_V E(B - V) = 0.13$ (see the blue curve in Fig. 3), which corresponds to a reduced $\chi^2 = 1.36$. This is slightly larger that 1 (corresponding to a perfect match) and certainly reflects the influence of the limitations listed above. Within a confidence interval of 68% (i.e., 1-σ for a Gaussian distribution), we found $Z = Z_\odot$, $\tau \in [0; 500]$ Myr, $t \in [0.13; 0.64]$ Myr, and $A_V \in [0; 0.28]$, while for a confidence interval of 90%, we found $Z \in [1.0; 2.5]\, Z_\odot$, $\tau \in [0; 3500]$ Myr, $t \in [0.06; 0.91]$ Myr, and $A_V \in [0; 0.74]$ (see Fig. 3). We note that a solar metallicity is further supported by the low resolution VIMOS spectrum retrieved from the VVDS archive (see Fig. 6).

We also note the presence of Balmer absorption lines in this best SED model, which suggests the presence of an underlying older stellar population (A/F stars). To quantify this further, we tried to fit an additional stellar population of old stars following the method described by Papovich et al. (2001): we generated SSPs with the same parameters that the best-fit SED except its age, which was set to be the age of the Universe at the redshift of the object (~7.5 Gyr). In principle, this allows us to constrain the maximal contribution of an older stellar population in terms of M/L that is still consistent with the data.

The result of the fit of this additional population is shown in Fig. 4. As expected, this additional old population influences the resulting SED only above 4000 Å, and particularly in the NIR. One might wonder whether this additional old population is real, given that the resulting combined SED does not seem to improve the global fit in this region, where the addition of such an older population, if real, should in principle lead to an improvement. This is due to the fact that we have not constrained the best mix between the young and old populations, but the maximal contribution of old stars to the best young population model (see above and Papovich et al. 2001), which is a more conservative approach. To quantify whether or not the addition of this older stellar population leads to a better SED fitting, we performed an F-test between the "old+young" model and the original "young" model. This test reveals that the addition of an older population does not give a significantly better representation of the observed SED, as also noticed by Papovich et al. (2001) in most of their more distant LBGs. Actually, constraining an old stellar population from the SED alone is not an easy task as these stars have a very modest contribution to the light: it is not surprising that trying to disentangle old stars from younger ones in an SED does not lead to conclusive results. Therefore, while there is no direct evidence for the presence of an older stellar population, its presence cannot be excluded either.

In conclusion, the SED fitting evidences that J033241.88-274853.9 is a relatively low-mass object, whose light is little impacted by dust, and dominated by a very young stellar population aged by a few hundreds of Myr. These stars appeared to be formed during a relatively short burst lasting less than a Gyr.

4. Stellar mass, SFR, and gas fraction

4.1. Stellar mass

Using the best-fit "young" model, the stellar mass was found to be $\log (M_{stellar}/M_\odot) = 9.45 \pm_{0.14}^{0.17}$ (90% confidence intervals). This is a factor ~8 smaller than the stellar mass derived in Paper III, using Bell et al. (2003) simplified prescription (see Annex of Paper III for detail), which can be easily explained by the very young age of J033241.88-274853.9: in this case, it is well known
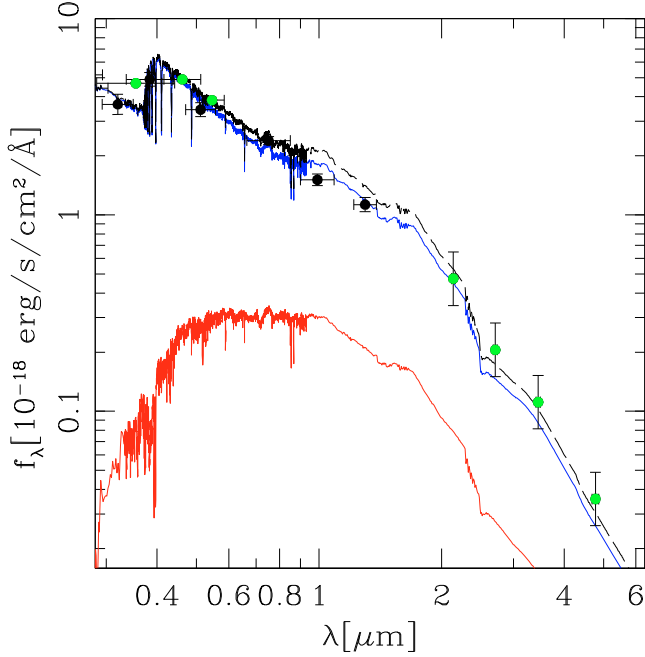
Fig. 4. Rest-frame SED of J033241.88-274853.9 for wavelengths above 4000 Å. The additional older population fitted together with the best-fit model (here in blue) is shown in red. The dashed-black line shows the sum of the two models.

that using such simplified prescription can lead to strongly overestimate the stellar mass (Bell et al. 2003). However, as discussed above, we cannot exclude the presence of old stars that could contribute substantially to the global stellar mass, even if they do not contribute significantly to the light. Considering the two stellar components model of Fig. 4, we find a total stellar mass of $\log(M_{\text{stellar}}/M_\odot) = 9.73$, with a contribution of the old stellar population of $\log(M_{\text{stellar}}/M_\odot) = 9.4$, i.e., roughly half of the total stellar mass. As the presence of this population remains hypothetical, we adopt the stellar mass corresponding to the "young" population model, and take this possible additional contribution into account in the error-bar, which leads us to $\log(M_{\text{stellar}}/M_\odot) = 9.45 \pm^{0.28}_{0.14}$.

4.2. Star formation rate

The 100-Myr average SFR was found to be $2.8^{+3.7}_{-2.8}$ $M_\odot$/yr, in good agreement with the estimate from the rest-frame magnitude at 2800 Å, i.e., $SFR \sim 3.3$ $M_\odot$/yr. Using the fitted extinction curve with $A_V = 0.13$ mag, we find $A_{2800} = 0.33$ mag, which in turn leads to a dust-corrected SFR of 4.47 $M_\odot$/yr. At this SFR, the mass doubling-time of J033241.88-274853.9 is found to be 0.63 Gyr, i.e., significantly lower than the age of the Universe at this redshift. This confirms that J033241.88-274853.9 formed its young stars quite rapidly, in a rather single burst of star formation as opposed to a more continuous star formation history. Finally, following Le Floc'h et al. (2005), we estimated that the detection limit of MIPS at 24 μm corresponds to $\sim$10 $M_\odot$/yr at $z \sim 0.65$, which is consistent with the non-detection of J033241.88-274853.9 in this band (see Sect. 3). We conclude that the SFR of J033241.88-274853.9 is therefore in the range 4.5−10 $M_\odot$/yr, if one takes into account both contributions from the UV and the IR.

4.3. Gas fraction

It is possible to estimate the gas fraction of J033241.88-274853.9 by forcing the galaxy to obey the Schmidt-Kennicutt relation between the star formation surface density and the gas surface density (Kennicutt 1998). Indeed, this relation seems to hold for all morpho-kinematic types (e.g., Di Matteo et al. 2007). We adapted the method used in Erb et al. (2006), to relate the gas mass surface density to the SFR surface density derived from the UV. Using the dust-corrected SFR will first provide us with a lower limit on the gas fraction, since we ignore the contribution from the re-processed light in the IR. We used the ACS half-light radius (assuming a total radius of two times the measured half light radius of 3.5 kpc, see Paper II) to derive the SFR per unit area, which is converted into a gas surface density using the Schmidt-Kennicutt relation (Kennicutt 1998). We then converted this gas mass surface density into a gas mass by estimating the maximal extent of [OII] emission from GIRAFFE data (see Fig. 2), quadratically deconvolved from the effect of a 0.8 arcsec seeing, which led us to $f_{\text{gas}} = 73\%$. Similarly, we estimated an upper limit to the gas fraction using the upper limit on the SFR of 10 $M_\odot$/yr, which gives $f_{\text{gas}} = 82\%$. We conclude that J033241.88-274853.9 is a very gas-rich galaxy with f_{gas} in the range 73−82%. We will discuss this point in the next section.

5. The J033241.88-274853.9 disk formation process

The gaseous phase of J033241.88-274853.9 is found to be rotating and turbulent (see Sect. 2). Because of the relatively coarse spatial resolution of the GIRAFFE IFU, it is not possible to derive accurately enough the exact geometry of the gaseous phase from the [OII] map alone. In this section, we examine two possible geometries for this gaseous phase, which corresponds to two distinct scenarios for the formation of the stellar disk.

5.1. Is J033241.88-274853.9 a collapsing gas-rich rotating disk?

The kinematical properties of the ionized gas suggests that the gaseous phase might be distributed into a rotating thick disk. In this scenario, this pre-existing gas-rich disk would have undergone a starburst event $\sim$320 Myr ago, partly collapsing into a young stellar disk.

If this case, then this galaxy should be dynamically relaxed and lie on the Tully-Fisher relation. However, the stellar mass derived from the SED fitting appears to be $\sim$5 times smaller than the one predicted by the stellar-mass Tully-Fisher Relation (smTFR) at $z \sim 0.6$ (Puech et al. 2008). On the one hand, this offset relative to the distant TFR could suggest that J033241.88-274853.9 is quite peculiar, as most of the outliers to the distant TFR usually lie *above* the relation (Puech et al. 2008). On the other hand, such an offset from the smTFR has been observed in local dwarf galaxies: because they have very large gas fractions, they lie below the smTFR. If one accounts for all baryons, then all galaxies follow the same "baryonic" TFR (bTFR, McGaugh 2005). To test if the large gas fraction of J033241.88-274853.9 (see Sect. 4) can be responsible for this shift relative to the TFR, we can derived the gas fraction needed for this galaxy to lie on the bTFR and see whether or not it is consistent with the range of f_{gas} derived in Sect. 4. Using the local smTFR as a proxy for the bTFR (McGaugh 2005), one can estimate the J033241.88-274853.9 gas fraction to be $\sim$91%, with a lower bound of $\sim$83% if ones takes into account the effect of a possible old stellar population. This lower limit is roughly compatible with the range of

value derived in Sect. 4. This means that the spectro-photometric properties of J033241.88-274853.9 are not inconsistent with a dynamical state of equilibrium, as expected from a relaxed rotating disk.

One has to explain the decoupling between the ionized gas and star distributions (see Sect. 2). Many scenarios have been proposed to explain gas and/or star lopsidedness in local galaxies, but to our knowledge, none of them appears able to explain a decorrelation between star and gas distribution such as the one observed in J033241.88-274853.9 (e.g., Mapelli et al. 2008). In order to check whether seeing effects and the coarse spatial sampling of GIRAFFE could explain this apparent decoupling, we used the degraded V-band ACS image constructed in Sect. 2 to estimate the amount of [OII] emission that could be spread out by seeing effects in the region encompassed by the leftmost GIRAFFE pixel. Indeed, assuming that J033241.88-274853.9 is a relaxed rotating disk, then one expects that at zero order, the rest-frame B-band (corresponding to the observed V-band) stellar and ionized gas distributions should be correlated. If one further assumes that the [OII] equivalent width is spatially constant, then comparing the GIRAFFE [OII] distribution to the smoothed ACS V-band image underpredicts the EW_0([OII]) in the leftmost pixel by a factor of 10: we find that the flux ratio between the region encompassed by the brightest GIRAFFE pixel (i.e., the GIRAFFE pixel corresponding to the dynamical center of rotation) and the region encompassed by leftmost GIRAFFE pixel is ten times larger than the same ratio directly measured in the GIRAFFE [OII] emission map. This would mean that photoionization can account for only $\sim$10% of the total EW_0([OII]) in this pixel. However, [OII] and rest-B fluxes trace star formation on different timescales, since [OII] traces only the youngest stars. Therefore, it could be possible to have a true [OII] equivalent width that varies spatially. Given the relatively coarse spatial resolution of GIRAFFE observations, it is likely that this does not qualitatively change the fact that, if J033241.88-274853.9 is a relaxed rotating disk, the dominant ionization source of the gas in its southern part remains to be explained.

The rotating disk model faces with another difficulty, which is the extension of the central peak of dispersion in the southern part (see Sect. 2). Indeed, the morphological analysis reveals no central bar, and there is no obvious correlation between the velocity dispersion in these regions and the color map. Therefore, this excess of velocity dispersion in this region remains also unexplained.

5.2. Is J033241.88-274853.9 a major merger remnant?

Another possibility is that the J033241.88-274853.9 gaseous phase is made of heated spiraling gas re-accreted after the final coalescence of a merger. Indeed, the merger scenario fits well with the burst duration and the SFR in this range of stellar mass (i.e., a few $M_\odot$/yr during a few hundreds of Myr, see, e.g., Cox et al. 2008, and their G0-G0 merger).

In such a scenario, the gas surrounding J033241.88-274853.9 would not be dynamically relaxed yet, and would rotate too fast for the underlying stellar mass. Such an effect has been observed in numerical simulations of mergers (see, e.g., Puech et al. 2007a). Therefore, this scenario also provides a reasonable explanation for the shift relative to the smTFR (see also discussion of "kinematic cooling" in Atkinson et al. 2007).

After the final coalescence of the two progenitors, the gas expelled away in tidal tails can relax by dynamical friction. At least part of this gas can be subsequently re-accreted and spirals around the merger remnant, which can mimic the kinematics

of a rotating thick disk at large spatial scales, as shown by Barnes (2002). Moreover, in principle, the large gas fraction of J033241.88-274853.9 is high enough to allow a disk to be rebuilt following the merger, as shown by Robertson et al. (2006). Such numerical simulation including star formation have demonstrated how a merger between two equal-mass, gas-rich disks could allow a stellar disk to reform with an angular momentum inherited from the orbital momentum of the progenitors (Robertson et al. 2006). Indeed, the specific angular momentum of the gas in J033241.88-274853.9 is found to be $j = 1120 \pm 255$ kpc km s^{-1}, very close to local gaseous disks (see Puech et al. 2007a).

As we have shown in the previous section, the lack of stars on the southern side of the galaxy implies that gas cannot be ionized by hot stars in this region. The low disk V/σ and the excess of velocity dispersion relative to a rotating disk model in this region (see Sect. 2) both suggest that the disk might be heated by shocks. These shocks could be produced by collisions between gaseous tidal tails formed during the merger. Such shocks could ionize the gas in this region, while also preventing star formation, which provides a very simple explanation of the decoupling between the gas and stars distributions. In absence of significant stellar light, gas continuum emission alone can indeed result in very high equivalent width, i.e., in the range 80–370 Å depending on electron density (Osterbrock & Ferland 2006): this can largely account for the observed EW_0([OII]) in the southern region of J033241.88-274853.9.

In order to test further the merger scenario, we looked in Barnes (2002) numerical simulations for similarities with the properties of J033241.88-274853.9. In Fig. 5, we show a snapshot of the gas distribution extracted from a simulation a major merger (i.e., mass ratio 1:1) of inclined disks on a parabolic orbit with a large pericentric separation ($r_{peri} = 0.4$, see Barnes 2002, for detail). This snapshot was extracted approximately 250 Myr after the final coalescence of the two progenitors, which is consistent with the age of the young stellar population derived in Sect. 3. Because the stellar light of J033241.88-274853.9 is dominated by young and intermediate aged stars (see Sect. 3), the gas concentration can be considered as tracing the distribution of new stars at very first order, which provides us with a useful comparison to J033241.88-274853.9. Indeed, in the central regions, the remnant gas is distributed into an asymmetric rotating disk (see the white ellipse). The gas expelled during the merger is re-accreted after the final coalescence through two spiraling tails (see outer-most white arrows). Shocks are clearly seen at the basis of the upper tail, which occur between the gas falling down from this tail onto the central region and the gas rotating around an asymmetric new disk. The initial gas fraction in the simulation is set to be 12.5% that of the stellar mass in the disk. It is interesting to note that in numerical simulations, the rotation support of the re-formed stellar disk after a major merger is an increasing function of the gas fraction (Robertson et al. 2006): with the gas fraction as the one inferred in J033241.88-274853.9 (see Sect. 4.3), one expects a strongly rotationally supported remnant stellar disk. The similarities between J033241.88-274853.9 and this simulation demonstrate the viability of the merger scenario.

6. Discussion and conclusion

If one assumes that J033241.88-274853.9 is a relaxed rotating disk, then its gas fraction must be unusually high. Indeed, locally, such large gas fractions are found only in the most extreme gas-rich dwarfs galaxies (Schombert et al. 2001): galaxies on the
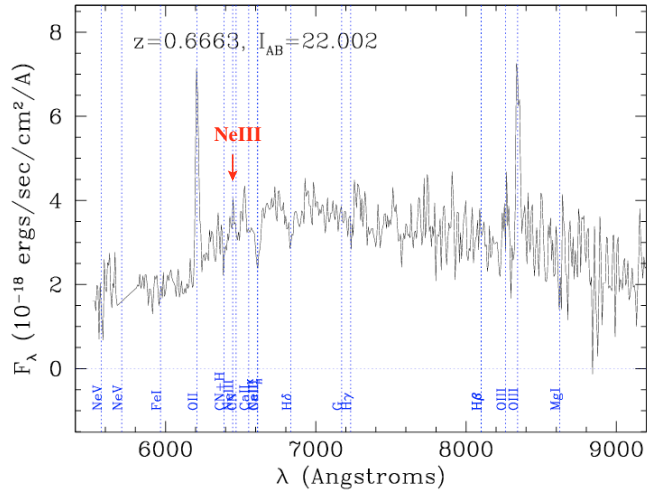
Table 2. Summary of the main characteristics of J033241.88-274853.9. A possible explanation for each property is given for the two scenarios discussed in the text.

Property	Starbursting Rotating Disk	Major Merger Remnant
Extension of the peak of dispersion in the southern part	Cause unknown	Heating due to shocks between the gas in tidal tails and the central regions
Decoupling between the distribution of the ionized gas & stars	Photo-ionization can account for only 10% of $EW_0([OII])$	Shocks can ionize the gas and account for 100% of $EW_0([OII])$, while preventing star formation
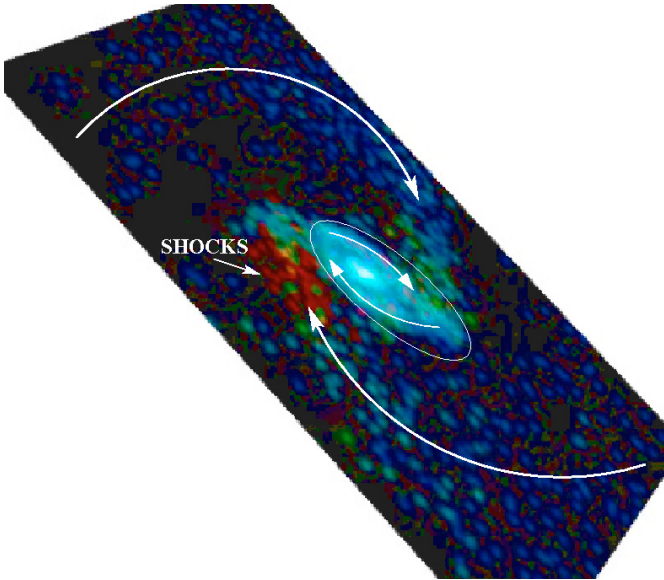
Fig. 5. Snapshot extracted from a simulation of a major merger by Barnes (2002). Only gas is shown, and colors indicate energy dissipated by shocks. The view has been rotated and inclined in order to qualitatively match the morpho-kinematics of J033241.88-274853.9.

Fig. 6. VIMOS spectrum of J033241.88-274853.9. We have directly reproduced the gif figure of this object (EIS ID No. 24025) as given by the VVDS database (see text). The expected position of the NeIII emission line is indicated in red.

blue sequence with a similar stellar mass have gas fraction significantly smaller (Kannappan 2004). At $z \sim 0.6$, such gas fractions appears to be also exceptional when compared to the average gas fraction (30%) estimated at this redshift by Liang et al. (2006). One has to look at significantly higher redshifts in order to find such large gas fractions in $\log(M_{\text{stellar}}/M_{\odot}) = 9.45$ galaxies (see, e.g., Erb et al. 2006 for $z \sim 2$ galaxies). However, it does not exclude that we might be observing the collapse of an exceptionally gas-rich rotating disk into stars.

In this case, one could expect the disk to fragment into clumps, as described by numerical simulations (e.g., Immeli et al. 2004; Bournaud et al. 2007). In this simulations, gaseous unstable disks can fragment into UV bright star-forming clumps with typical sizes ~1 kpc. One can note in Fig. 1 the presence of several blue regions in the disk, which might suggest that the gaseous phase of J033241.88-274853.9 is indeed fragmented into clumps, as the size of these regions is found to match that expected in such clumps (see Fig. 1). Moreover, this fragmentation process is expected to occur after 100−300 Myr and to last ~0.5−1.0 Gyr, which might also fit well with the age inferred above for J033241.88-274853.9. Such models have also been shown to reproduce the lopsidedness of distant clump systems, provided that a disk-halo offset is introduced at the beginning of the simulation (Bournaud et al. 2008). However, even with such initial asymmetries, the resulting gas and stars distributions appear to be relatively well correlated, which is clearly at odd with the observed decoupling.

Another important argument is the lack of photo-ionization flux in the southern part of J033241.88-274853.9 to account for the whole $EW_0([OII])$ measured in this region, while in the major merger hypothesis, ionization by shocks can easily account for the whole $EW_0([OII])$. To look for further evidence of the presence of shocks, we retrieved from the VVDS archive[2] an integrated VIMOS spectrum of J033241.88-274853.9, which is reproduced in Fig. 6 (Le Fèvre et al. 2005). This spectrum shows some faint but very likely emission at $\lambda_{\text{rest}} = 3869$ Å, which could correspond to the NeIII emission line. This strengthens the presence of ionizing shocks in this galaxy (Osterbrock & Ferland 2006).

In the previous and present sections, we have identified and discussed two very unusual properties of J033241.88-274853.9, which are the decoupling between the distributions of stars and gas, and the excess of velocity dispersion in the southern part. We have summarized them in Table 2, along with their respective possible explanation depending on the two disk formation scenarios considered. Both properties would require further assumptions to be explained in the frame of a collapsing gas-rich rotating disk scenario, while they find a natural and unique explanation through shock-induced ionization in the frame of the merging of two gas-rich galaxies.

---

[2] http://cencosw.oamp.fr/

References

Arnouts, S., Vandame, B., Benoist, C., et al. 2001, A&A, 379, 740
Atkinson, N., Conselice, C. J., & Fox, N. 2007, MNRAS, submitted [arXiv:0712.1316]
Avni, Y. 1976, ApJ, 210, 642
Barnes, J. E. 2002, MNRAS, 333, 481
Beckwith, S. V. W., Stiavelli, M., & Koekemoer, A. M. 2006, AJ, 132, 1729
Bell, E. F., McIntosh, D. H., Katz, N., & Weinberg, M. D. 2003, ApJS, 149, 289
Bertin, E., & Arnouts, S. 1996, A&AS, 117, 393
Bournaud, F., Elmegreen, B. G., & Elmegreen, D. M. 2007, ApJ, 670, 237
Bournaud, F., Daddi, E., Elmegreen, B. G., et al. 2008, A&A, 486, 741
Bruzual, G. A. 2007, From stars to galaxies: building the pieces to build up the Universe, ed. A. Vallenari, R. Tantalo, L. Portinari, & A. Moretti, ASP Conf. Ser. [arXiv:astro-ph/0702091]
Calzetti, D., Armus, L., Bohlin, R. C., et al. 2000, ApJ, 533, 682
Cardelli, J. A., Clayton, G. C., & Mathis, J. S. 1989, ApJ, 345, 245
Cox, T. J., Jonsson, P., Somerville, R., et al. 2008, MNRAS, 384, 386
Di Matteo, P., Combes, F., Melchior, A.-L., et al. 2007, A&A, 468, 61
Erb, D. K., Steidel, C. C., Shapley, A. E., et al. 2006, ApJ, 646, 107
Fitzpatrick, E. L. 1999, PASP, 111, 63
Fitzpatrick, E. L., & Massa, D. 2007, ApJ, 663, 320
Giacconi, R., Zirm, A., Wang, J., et al. 2002, ApJS, 139, 369
Hammer, F., Flores, H., Elbaz, D., et al. 2005, A&A, 430, 115
Hammer, F., Puech, M., Chemin, L., et al. 2007, ApJ, 662, 322
Hopkins, P. F., Cox, T. J., Younger, J. D., & Hernquist, L. 2008, ApJ, submitted [arXiv:0806.1739]
Immeli, A., Samland, M., Gerhard, O., & Westera, P. 2004, A&A, 413, 547
Kannappan, S. J. 2004, ApJ, 611, 89

Kennicutt, R. 1998, ARA&A, 36, 189
Le Fèvre, O., Vettolani, G., Garilli, B., et al. 2005, A&A, 439, 845
Le Floc'h, E., Papovich, C., Dole, H., et al. 2005, ApJ, 632, 169
Liang, Y. C., Hammer, F., & Flores, H. 2006, A&A, 447, 113
Lotz, J., Jonsson, P., Cox, T. J., & Primack, J. R. 2008, ApJ, submitted [arXiv:0805.1246]
Mapelli, M., Moore, B., & Bland-Hawthorn, J. 2008, MNRAS, in press [arXiv:0805.1104]
Mayer, L., Governato, F., & Kaufmann, T. 2008, Adv. Sci. Lett., in press [arXiv:0801.3845]
McGaugh, S. S. 2005, ApJ, 632, 859
Morrissey, P., Conrow, T., Barlow, T. A., et al. 2007, ApJS, 173, 682
Neichel, B., Hammer, F., Puech, M., et al. 2008, A&A, 484, 159
Osterbrock, D. E., & Ferland, G. J. 2006, Astrophysics of gaseous nebulae and active galactic nuclei, 2nd Ed., ed. D. E. Osterbrock, & G. J. Ferland (Sausalito, CA: University Science Books)
Papovich, C., Dickinson, M., & Ferguson, H. C. 2001, ApJ, 559, 620
Peng, C. Y., Ho, L. C., Impey, C. D., et al. 2002, AJ, 124, 266
Puech, M., Hammer, F., Lehnert, M. D., & Flores, H. 2007a, A&A, 466, 83
Puech, M., Hammer, F., Flores, H., et al. 2007b, A&A, 476, L21
Puech, M., Flores, H., Hammer, F., et al. 2008, A&A, 484, 173
Ravikumar, C. D., Puech, M., Flores, H., et al. 2007, A&A, 465, 1099
Robertson, B., Bullock, J. S., Cox, T. J., et al. 2006, ApJ, 645, 986
Rosati, P., Tozzi, P., Giacconi, R., et al. 2002, ApJ, 566, 667
Salpeter, E. E. 1955, ApJ, 121, 161
Schombert, J. M., McGaugh, S. S., & Eder, J. A. 2001, ApJ, 121, 2420
Yang, Y., Flores, H., Hammer, F., et al. 2007, A&A, 477, 789
Wuyts, S., Labbé, I., Forster-Schreiber, N. M., et al. 2008, ApJ, in press [arXiv:0804.0615]